

# SCIENTIFIC REPORTS



OPEN

## Layer-specific potentiation of network GABAergic inhibition in the CA1 area of the hippocampus

Michelangelo Colavita<sup>1,2,3</sup>, Geoffrey Terral<sup>1,2</sup>, Clement E. Lemercier<sup>1,2</sup>, Filippo Drago<sup>3</sup>, Giovanni Marsicano<sup>1,2,#</sup> & Federico Massa<sup>1,2,#</sup>

Received: 21 October 2015

Accepted: 03 June 2016

Published: 27 June 2016

One of the most important functions of GABAergic inhibition in cortical regions is the tight control of spatiotemporal activity of principal neuronal ensembles. However, electrophysiological recordings do not provide sufficient spatial information to determine the spatiotemporal properties of inhibitory plasticity. Using Voltage Sensitive Dye Imaging (VSDI) in mouse hippocampal slices, we demonstrate that GABA<sub>A</sub>-mediated field inhibitory postsynaptic potentials undergo layer-specific potentiation upon activation of metabotropic glutamate receptors (mGlu). VSDI recordings allowed detection of pharmacologically isolated GABA<sub>A</sub>-dependent hyperpolarization signals. Bath-application of the selective group-I mGlu receptor agonist, (S)-3,5-Dihydroxyphenylglycine (DHPG), induces an enhancement of the GABAergic VSDI-recorded signal, which is more or less pronounced in different hippocampal layers. This potentiation is mediated by mGlu<sub>5</sub> and downstream activation of IP<sub>3</sub> receptors. Our results depict network GABAergic activity in the hippocampal CA1 region and its sub-layers, showing also a novel form of inhibitory synaptic plasticity tightly coupled to glutamatergic activity.

In the mammalian brain, the main source of inhibition is provided by the neurotransmitter gamma-aminobutyric acid (GABA), which acts on two classes of receptors: the ionotropic GABA<sub>A</sub> and the metabotropic GABA<sub>B</sub><sup>1</sup>.

In cortical areas, GABA is released by locally projecting interneurons, which are estimated to account for approximately 11% of the total cell population in the hippocampal CA1 region<sup>2,3</sup>. However, despite the paucity of these cells within this region, each interneuron can make synapses with several hundreds of pyramidal cells<sup>4</sup> and other interneurons<sup>4,5</sup>, providing an extremely complex and powerful spatiotemporal control of network activity.

At least 21 different classes of interneurons have been described in the CA1, classified on the basis of firing patterns, molecular expression profiles, and innervation properties<sup>4,6,7</sup>. This high morpho-physiological heterogeneity, together with the high degree of synaptic connectivity between pyramidal cells and other interneurons, suggest the existence of a “network of interneurons” with a key role in controlling hippocampal computations<sup>5,8,9</sup>. For instance, GABAergic cells through the release of GABA and subsequent activation of GABA<sub>A</sub> receptors hyperpolarize pyramidal cells<sup>10</sup>. Thus, depending on the wiring scheme of interneurons onto principal cells, feedback and/or feed forward inhibition may occur, which are fundamental processes in shaping the spatial and temporal profile of principal cell firing and global network activity<sup>11–13</sup>.

Moreover, the existence of GABAergic synapses between different types of interneurons<sup>14,15</sup>, including specialized interneuron-specific cells<sup>4,5</sup>, suggests that the inhibitory control of other interneurons is crucial in providing a higher level of coordination of hippocampal network activity<sup>5</sup>.

Due to technical limitations, such as the difficulty to obtain reliable electrophysiological recordings of local “inhibitory fields” by standard electrophysiological approaches<sup>16–18</sup>, very little is known concerning the global network activity and dynamics of interneurons. Indeed, powerful single-cell recordings, widely used to study the roles of inhibitory activity at the single cell level, is not appropriate to observe the global spatiotemporal patterns of activity of inhibitory networks. Such a “mesoscopic” level of analysis of local inhibitory systems is, therefore, a lacking element in the quest for understanding dynamics and properties of principal networks.

<sup>1</sup>INSERM U1215, NeuroCentre Magendie, AVENIR Group “Endocannabinoids and Neuroadaptation”, 33077 Bordeaux, France. <sup>2</sup>Université de Bordeaux, 33077 Bordeaux, France. <sup>3</sup>University of Catania, Biometec – Department of Biomedical and Biotechnological Sciences, 95125 Catania, Italy. <sup>#</sup>These authors jointly supervised this work. Correspondence and requests for materials should be addressed to F.M. (email: federico.massa@inserm.fr)

Voltage sensitive dye imaging (VSDI) allows coincident optical monitoring of neuronal activity within a wide range of spatial resolution (from very small cell compartments such as dendrites, to areas of several mm<sup>2</sup>), at millisecond time scale<sup>19,20</sup>. After binding cell membranes, voltage-sensitive dye molecules emit fluorescence proportionally to changes in membrane potential<sup>21</sup>. VSDI has been widely used to study excitatory network activity and single cell properties of neurons<sup>22–24</sup>. Notably, at regional (mesoscopic) level, VSDI allows for the dissection of depolarization signals within different anatomical compartments (e.g., hippocampal sub-layers). However, this feature of VSDI has not yet been used to characterize, pharmacologically and anatomically, the activity and plasticity of inhibitory networks.

Group-I metabotropic glutamate receptors (group-I mGlu receptors) include mGlu<sub>1</sub> and mGlu<sub>5</sub><sup>25</sup>. They constitute a subclass of metabotropic glutamate receptors that are coupled to G<sub>q</sub> heterotrimeric G proteins, thus leading to activation of phospholipase C and subsequent mobilization of inositol 1,4,5-trisphosphate (IP<sub>3</sub>), which in turn increases cytosolic Ca<sup>2+</sup> via activation of IP<sub>3</sub> receptors on the endoplasmic reticulum<sup>26</sup>. Activation of group-I mGlu receptors is known to strongly impact on synaptic properties and plasticity of hippocampal circuits<sup>27,28</sup>.

In this study, we took advantage of the VSDI technique to visualize and quantify evoked field inhibitory postsynaptic potentials (fIPSPs) in the CA1 hippocampal region, and to analyze their temporal and spatial features within the different sub-layers. In addition, we found that activation of mGlu<sub>5</sub> leads to an IP<sub>3</sub>-dependent potentiation of fIPSPs in a sub-region specific manner. These findings demonstrate the spatial and temporal distribution of GABAergic activity in the CA1 region of hippocampus and, most importantly, they show that metabotropic glutamatergic signaling bears a strong impact on the global and local activity of inhibitory networks in specific brain regions.

## Results

**GABA<sub>A</sub>-mediated network activity in the hippocampal CA1.** Stimulation of Schaffer's collateral pathway in hippocampal slices stained with Di-4-ANEPPS in drug-free ACSF produces a depolarization spanning along the horizontal axis of CA1 (Fig. 1a; green to red color-scale; Supplementary Video S1). To quantify depolarization-mediated VSDI signal, we drew a region of interest (ROI) covering the whole CA1 (Fig. 1b) and the resulting mean  $\Delta F/F^{-1}$  values over time are shown as an upward deflection of the signal lasting approximately 30 milliseconds (Fig. 1b, trace). More detailed analysis of VSDI-recorded depolarization revealed detectable signal specifically in the different layers of CA1, due to action potentials spreading along pyramidal cells (Fig. 1c, representative ROIs arrangement and corresponding traces). Consistent with previous reports under similar conditions<sup>23,29</sup>, these images represent the spreading of depolarization signals within the CA1 region. Next, we examined whether a GABAergic component could be identified in these VSDI recordings. Application of the GABA<sub>A</sub> receptor antagonist Picrotoxin (100 μM) induced an increase in the intensity of evoked depolarization signals both in the whole CA1 (Fig. 1d–f, Supplementary Video S2; AUC: baseline, 3 ± 0.2; PTX, 7.5 ± 2.4; p = 0.0068 baseline vs PTX, paired *t* test) as well as in the different sub-fields (Supplementary Fig. S1). Thus, VSDI depolarization signals result from the simultaneous activation of excitatory and inhibitory networks. To study in detail this GABAergic component of network activity, we isolated inhibitory neurotransmission by applying a cocktail of AMPA/Kainate and NMDA receptors antagonists (NBQX 10 μM and APV 50 μM respectively). This treatment fully abolished the depolarization signals in the whole CA1 and each CA1 sub-region (Fig. 1g–i; Supplementary Video S3), confirming their glutamatergic ionotropic origins. Importantly, however, blockade of ionotropic glutamatergic receptors also revealed a clear downward deflection of the traces below background fluorescence levels, which lasted approximately 200–250 milliseconds and was compatible with a hyperpolarizing event (Fig. 1g–i; blue color scale; Supplementary Video S3). Thus, stimulation of Schaffer's collaterals induces reliable and quantifiable hyperpolarizing field signals (hereafter called fIPSPs, i.e. field inhibitory postsynaptic potentials) in the CA1 region of the hippocampus.

Next, we set to characterize the nature of these hyperpolarization signals. First, input/output experiments revealed that evoked fIPSPs depend on the intensity of the stimulation, reaching a plateau level at 15–20 Volts (Fig. 2a), suggesting that they rely on neuronal activity. The application of the voltage-gated Na<sup>+</sup> channel blocker Tetrodotoxin (TTX, 1 μM) fully abolished fIPSPs in the whole CA1 (Fig. 2b, AUC: baseline, 7.8 ± 0.9; TTX, 2.3 ± 0.3; background, 2.6 ± 0.3; p = 0.0002 baseline vs TTX, paired *t* test; p = 0.5177 TTX vs background, unpaired *t* test) and in all hippocampal sub-regions (Supplementary Fig. S2) reducing them to basal background levels (see Methods for background definition). Thus, VSDI-recorded fIPSPs are not due to artifacts and depend on neuronal activity.

The main neurotransmitter mediating hyperpolarization in the brain is GABA, acting at ionotropic GABA<sub>A</sub> or metabotropic GABA<sub>B</sub> receptors<sup>1</sup>. Application of the GABA<sub>A</sub> receptor antagonist Picrotoxin (PTX, 100 μM) abolished fIPSPs signal in the whole CA1 region (Fig. 2c; AUC: baseline, 8.0 ± 0.7; PTX, 1.4 ± 0.4; background, 1.8 ± 0.7; p = 0.0014 baseline vs PTX, paired *t* test; p = 0.6610 PTX vs background, unpaired *t* test). Conversely, the GABA<sub>B</sub> receptor antagonist CGP55845 (5 μM) did not significantly alter CA1 fIPSPs (Fig. 2d; AUC: baseline, 9.3 ± 1.3; CGP55845, 8.1 ± 1.9; background, 1.1 ± 0.1; p = 0.3545 baseline vs CGP55845, paired *t* test; p = 0.01 CGP55845 vs background, unpaired *t* test), suggesting a specific involvement of GABA<sub>A</sub> receptors in the observed network hyperpolarization. This was further confirmed by the application of the positive allosteric modulator of GABA<sub>A</sub> receptor Chlordiazepoxide (CDP, 5 μM), which slightly but significantly increased fIPSPs amplitudes (Fig. 2e; AUC: baseline, 5.7 ± 0.9; CDP, 7.3 ± 0.9; background, 1.3 ± 0.3; p = 0.0320 Baseline vs CDP, paired *t* test; p < 0.0001 CDP vs Background, unpaired *t* test). Importantly, similar results were obtained when specific CA1 sub-regions were analyzed (Supplementary Fig. S2), further confirming the reliable nature of the observed VSDI signals as GABA<sub>A</sub> receptor-dependent synaptic hyperpolarization events. Thus, VSDI allows detection and quantification of activity-dependent hyperpolarization events in the CA1 hippocampal region after stimulation of a large network of GABAergic interneurons.

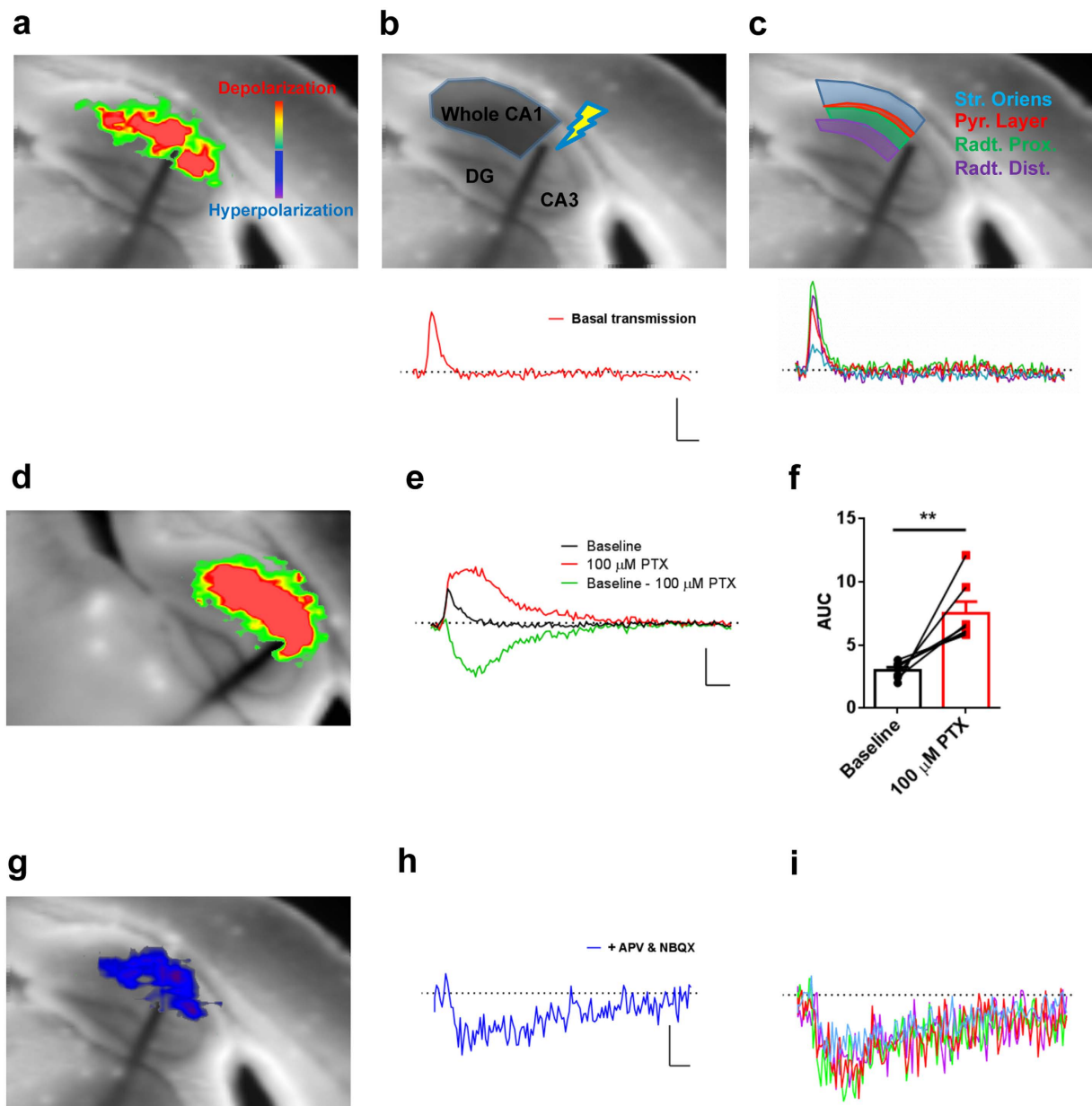


**Figure 1. Blockade of ionotropic glutamatergic transmission reveals network hyperpolarization throughout CA1.** (a) Representative frame showing VSDI-recorded depolarization activity after stimulation of Schaffer's collateral in drug-free ACSF. Inset color scale indicates depolarization (green to red) and hyperpolarization (blue to purple). (b,c) Representative regions of interest (ROIs) arrangement (upper panels) and corresponding traces (lower panels) showing resulting average VSDI-recorded depolarization in drug-free ACSF from a ROI covering the whole CA1 (b) and in its different sub-regions (c). Str. Oriens = *stratum oriens*, Pyr. Layer = Pyramidal Layer, Radt. Prox. = *radiatum proximal*, Radt. Dist. = *radiatum distal*. (d) Representative frame showing VSDI-recorded depolarization activity after stimulation of Schaffer's collateral following application of Picrotoxin (PTX, 100  $\mu$ M). (e) Representative traces showing the impact of GABAergic transmission on VSDI-recorded depolarization from a ROI covering the whole CA1 before (Baseline) and after application of PTX. The GABAergic component (Baseline - 100  $\mu$ M Picrotoxin) is obtained from the difference between Baseline and PTX conditions, respectively. (f) Quantification through area under curve (AUC) calculation of VSDI-recorded depolarization in the whole CA1 before (Baseline) and after application of PTX.  $n = 7$  slices from 5 mice. Bars represent mean  $\pm$  s.e.m. whereas over imposed lines are single values.  $**p < 0.01$ , two-tailed paired  $t$ -test. (g) Representative frame showing VSDI-recorded hyperpolarization activity after stimulation of Schaffer's collateral in presence of blockers of ionotropic glutamatergic transmission (APV & NBQX). (h,i) Representative traces showing VSDI-recorded hyperpolarization activity following APV & NBQX application from a ROI covering the whole CA1 (h) and in its different sub-regions (i). Scale bars are 25 milliseconds on X-axis and 0.2%  $\Delta F/F^{-1}$  on y-axis for traces in (b,c,e) whereas 0.05%  $\Delta F/F^{-1}$  on y-axis for traces in (h,i).

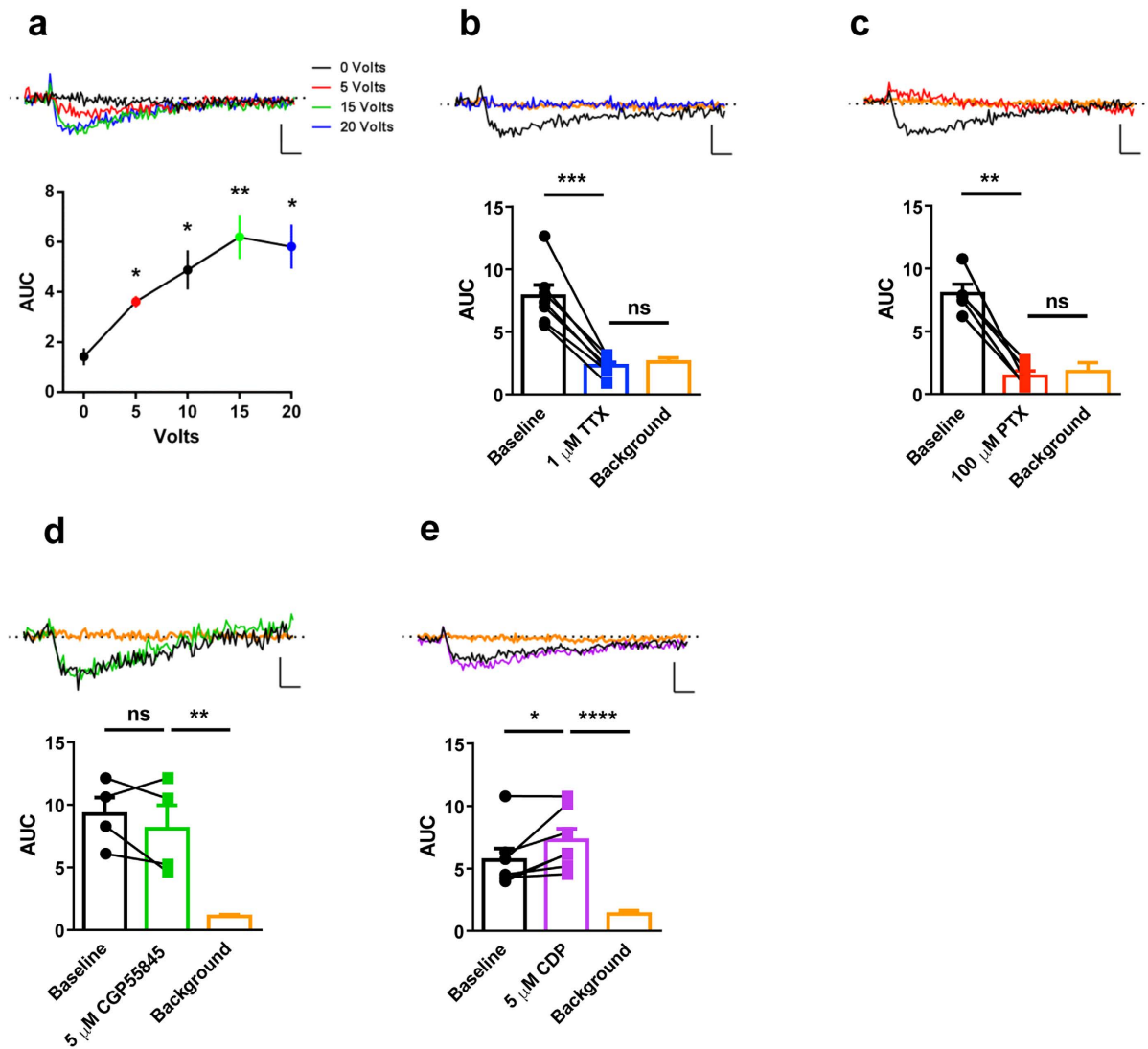


**Figure 2. Characterization of the VSDI-recorded fIPSPs.** (a) Increasing stimulation intensity every 5 minutes time steps significantly enhances the signal compared to 0 Volts [lower panel, one-way ANOVA with repeated measures over stimulation intensities ( $F_{(2,605,13,02)} = 12,95$ ,  $p = 0.0005$ ) followed by Tukey *post-hoc* test.  $n = 6$  slices from 5 mice]. (b) 1  $\mu$ M Tetrodotoxin (TTX) significantly abolishes the signal, which is statistically not different from the background, lower panel,  $n = 7$  slices from 5 mice. (c) 100  $\mu$ M Picrotoxin (PTX) significantly abolishes the signal, which is then not different from background, lower panel,  $n = 5$  slices from 3 mice. (d) 5  $\mu$ M CGP55845 does not affect the hyperpolarization signal, lower panel,  $n = 4$  slices from 2 mice. (e) 5  $\mu$ M Chlordiazepoxide (CDP) significantly increases the signal, lower panel,  $n = 7$  slices from 4 mice. In all graphs, signal of interest has been assessed in a ROI covering the whole CA1. In all figures, traces in upper panels are the average of traces from each experimental condition. Bars (b–e) and points (a) represent mean  $\pm$  s.e.m. whereas over imposed lines (b–e) are single values. Statistical significance has been assessed with two-tailed paired *t*-test between baseline condition and drug application, while two-tailed unpaired *t*-test has been used between drug application and respective background (b–e). Scale bars are 25 milliseconds on X-axis and 0.05%  $\Delta F/F^{-1}$  on Y-axis. \* $p < 0.05$ , \*\* $p < 0.01$ , \*\*\* $p < 0.001$ , \*\*\*\* $p < 0.0001$ , ns = not significant.

**Spatial distribution of network GABA<sub>A</sub> - mediated optical signals.** Unlike to classical electrophysiological recordings, the VSDI technique allows simultaneously observing synaptic events in different sub-regions of the area under investigation. Thus, we next quantified how the hyperpolarization signals induced by electrode stimulation are distributed among different CA1 sub-regions. Quantification of activity in equal ROIs distributed along the dorso-ventral axis of the CA1 region (Fig. 3a,b, see Methods) revealed that the strongest hyperpolarization was present in the CA1 pyramidal layer, whereas the *strata oriens* and *radiatum* (proximal and distal) displayed signals of lower amplitude (Fig. 3c,d). This observation is consistent with the fact that the majority of GABAergic synapses are located in the perisomatic area of CA1 pyramidal cells<sup>2,30</sup>.

Conversely, the intensity of the hyperpolarization signals decreased along the proximo-distal axis of CA1 (Fig. 3a,e–g), becoming undistinguishable from background levels at the most distal observed area (Fig. 3f,g).

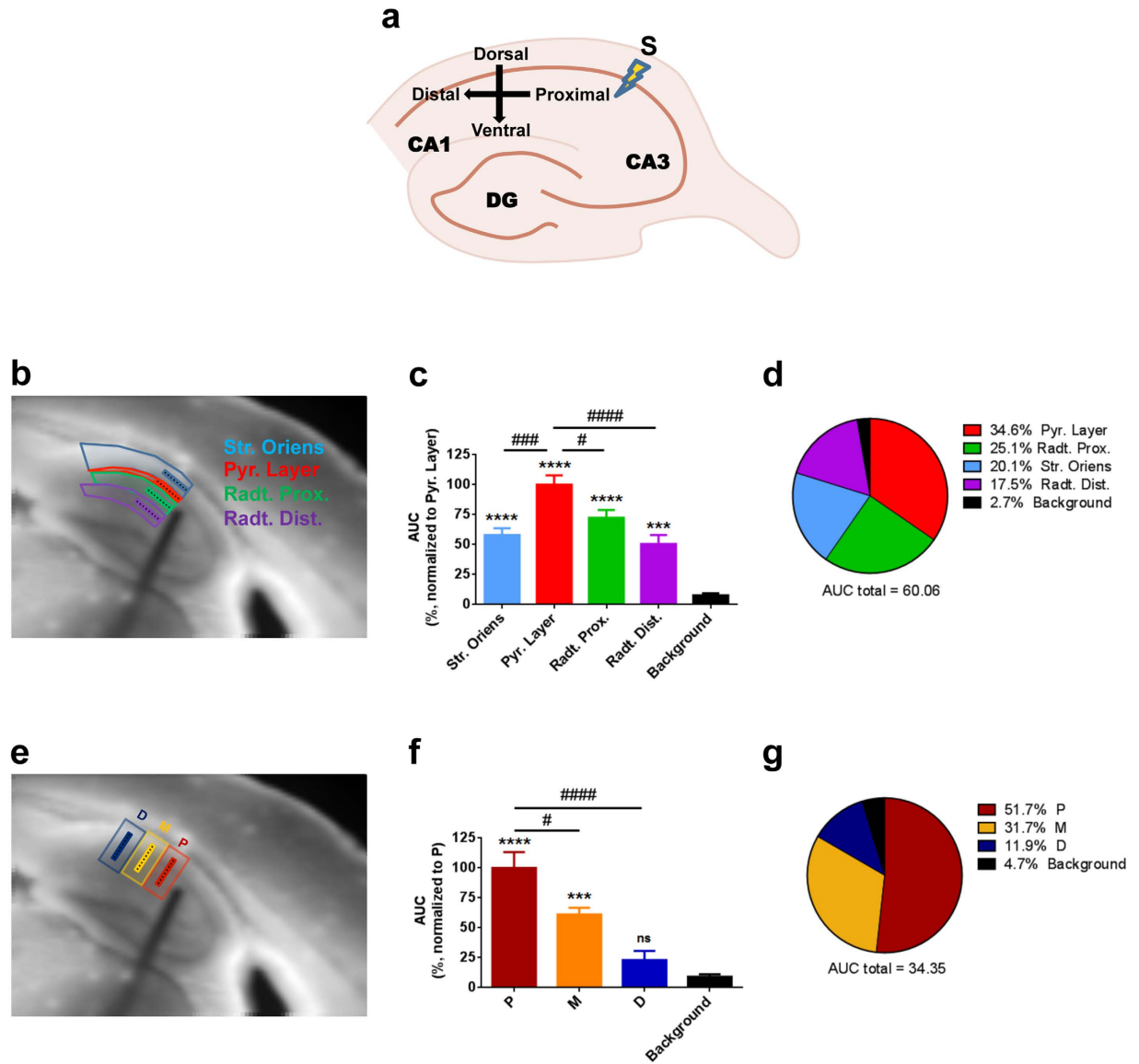


**Figure 3. Spatial distribution of VSDI-recorded fIPSPs throughout CA1 region.** (a) Cartoon representing the orientation of the different sub-regions studied in the CA1 (S, stimulation electrode). (b) Scheme showing spatial organization of the 8 pixels long ROI lines inside the dorso-ventral axis of CA1 (reference CA1 sub-regions are delimited by the colored contour). (c) Quantification through AUC of hyperpolarization from the ROI lines shows detectable signal in all the dorso-ventral regions of CA1, which is mainly localized in the pyramidal layer (one-way ANOVA followed by Tukey *post-hoc* test; asterisks are differences vs. “Background”, while hashes are differences vs. “Pyramidal layer”). (d) Pie chart summarizing the distribution of the signal from the lines along the dorso-ventral part of CA1 showing a predominant presence in the pyramidal layer (percentage of each region respect to the total AUC). (e) Scheme showing spatial organization of the 8 pixels long ROI lines inside the proximo-distal axis of CA1 (reference proximo-distal ROIs are delimited by the colored contour); “P” = proximal, “M” = medial, “D” = distal; distances from stimulation electrode are ~106, ~318 and ~531  $\mu\text{m}$  for regions P, M and D respectively. (f) Quantification through AUC of hyperpolarization from the ROI lines shows detectable signal at the proximity of the stimulation electrode (lines in regions “P” and “M”) while signal from lines in region “D” is not different from background (one-way ANOVA followed by Tukey *post-hoc* test; asterisks are differences vs. “Background”, while hashes are differences vs. “P”). (g) Pie chart summarizing how the signal from the ROI lines along the proximo-distal part of CA1 is concentrated in the proximity of the stimulation electrode (percentage of each region respect to the total AUC).  $n = 10$  slices from 10 mice. Data are mean  $\pm$  s.e.m. # $p < 0.05$ , ### and \*\*\* $p < 0.001$ , #### and \*\*\*\* $p < 0.0001$ , ns = not significant.

which were therefore excluded from further evaluations. These data indicate that the stimulation induces significant activation of the CA1 inhibitory network up to a distance of approximately 300–400  $\mu\text{m}$  relative to the stimulation electrode, consistent with previous data obtained by single cell recordings<sup>31</sup>. Thus, electrical stimulation in

the Schaffer's collaterals region can activate a large population of CA1 interneurons, of which a relative majority appears to form perisomatic innervation of pyramidal cells.

**Group-I mGlu receptors activation potentiates network hyperpolarization.** Group-I mGlu receptors have profound impact on neuronal activity, both on glutamatergic and GABAergic transmission<sup>27</sup>. In particular, field electrophysiological recordings of excitatory postsynaptic potentials (fEPSPs) showed that activation of group-I mGlu receptors decreases network excitatory transmission in the hippocampus and several other brain regions<sup>27,32</sup>. The study of metabotropic glutamatergic signaling on GABAergic activity, however, has been limited to date to single-cell recording settings<sup>33–40</sup>, with no studies focusing on network inhibition.

The application of the selective group-I mGlu receptor agonist (S)-3,5-Dihydroxyphenylglycine (DHPG, 50  $\mu$ M, 10 minutes) led to a persistent enhancement of VSDI-recorded evoked fEPSPs in the whole CA1 region as compared to control conditions, which lasted beyond washout of the drug (Fig. 4a).

A closer dissection of the sub-regional fEPSPs distribution revealed that this effect of DHPG was present in different layers and in proximal and medial regions relative to the stimulation electrode (Fig. 4b). Interestingly, however, the DHPG effect differed in amplitude and duration in the different sub-regions analyzed. The magnitude was greatest in the proximal *stratum radiatum*, and minimal in the *stratum oriens* and pyramidal layer (Fig. 4b–h). Time-course analyses showed that the effect of DHPG lasted up to 60 minutes in the whole CA1 region (Fig. 4a), which was likely due to the impact of the proximal *stratum radiatum* (Fig. 4e). In contrast, the DHPG-induced potentiation of fEPSPs was of shorter duration in the pyramidal layer and distal *stratum radiatum* (Fig. 4d,f, 20 min). In the *stratum oriens*, two-way ANOVA analysis revealed a significant treatment effect ( $F_{(1,60)} = 6.934$ ,  $p = 0.0107$ ), without “time x treatment” interaction, impeding the *post-hoc* determination of the time-dependent impact of DHPG (Fig. 4c). On the longitudinal axis, the amplitude of DHPG effect was not significantly different between areas located proximal or distal to the stimulation electrode (Fig. 4b). However, the DHPG-induced potentiation of fEPSPs was longer lasting in the CA1 portion closer to the electrode (Fig. 4g).

In addition, we tested if different doses and durations of DHPG application could also trigger a long-lasting increase in VSDI-recorded fEPSPs. As shown in Supplementary Fig. S3, DHPG application at half the previous concentration and for half the previous duration was sufficient to induce a persistent potentiation of network GABAergic activity in the whole CA1.

**mGlu<sub>5</sub> mediates DHPG-induced potentiation of fEPSPs.** As DHPG activates both mGlu<sub>1</sub> and mGlu<sub>5</sub>, we asked if either or both of these receptors are involved in the fEPSPs potentiation. Pretreatment of the slices with the specific mGlu<sub>1</sub> antagonist LY367385 (100  $\mu$ M) did not alter the effect of DHPG in the CA1 region (Fig. 5a). In contrast, the application of the specific mGlu<sub>5</sub> antagonist MPEP (25  $\mu$ M) fully blocked the DHPG-induced potentiation of fEPSPs (Fig. 5a). Importantly, when applied right after DHPG, MPEP was unable to block the potentiation of fEPSPs, showing that transient activation of mGlu<sub>5</sub> receptors induces a genuine phenomenon of GABAergic synaptic plasticity, which is not due to lack of DHPG washout. Thus, activation of mGlu<sub>5</sub> receptors is necessary for the induction but not for the maintenance of this plasticity.

At sub-regional level, similar results were obtained, with the exception of the *stratum oriens*, where, due to the weak effect of DHPG (see Fig. 4c), the data displays only non-significant trends (Fig. 5b). Thus, LY367385 did not alter the DHPG effect in any sub-region analyzed (Fig. 5c–g), whereas MPEP blocked this effect in all areas if applied before and not after DHPG (Fig. 5c–g). These data show that DHPG-induced potentiation of fEPSPs in different CA1 hippocampal sub-regions shares the same mechanisms, which rely on activation of mGlu<sub>5</sub> receptors.

**Role of IP<sub>3</sub> intracellular receptors.** Activation of mGlu<sub>5</sub> triggers G<sub>q</sub> protein signaling, which, *via* the inositol 1,4,5-trisphosphate cascade, ultimately leads to the recruitment of the ligand-gated Ca<sup>2+</sup> release channels IP<sub>3</sub> receptors in the endoplasmic reticulum (ER) and the increase of cytosolic Ca<sup>2+</sup><sup>26,41</sup>. Therefore, we asked whether IP<sub>3</sub> receptors are involved in the DHPG-induced potentiation of fEPSPs in the CA1 hippocampal region. Application of DHPG in continuous presence of the membrane permeable IP<sub>3</sub> receptor antagonists 2-APB or Xestospongin C failed to increase VSDI-recorded hyperpolarization in the whole CA1 and in all the sub-regions analyzed (Fig. 6a–g), clearly pointing to the involvement of intracellular IP<sub>3</sub> receptors in this effect.

## Discussion

This study shows that VSDI is a suitable technology to investigate network inhibitory activity in hippocampal slices, providing an equivalent of “field inhibitory postsynaptic potentials”, which depend on neuronal activity and are inhibited or potentiated by antagonism or allosteric enhancement of GABA<sub>A</sub> receptors, respectively. As compared to classical electrophysiological techniques, a clear advantage of this approach is that it preserves spatial information, enabling the opportunity to dissect the intensity and distribution of fEPSPs amongst different sub-regions of a given brain area. Like other techniques, VSDI presents also specific drawbacks, such as the relative low levels of signal-to-noise ratio<sup>19,20</sup>, which is particularly evident when inhibitory field potentials are observed. However, the fact that the hyperpolarization observed in our study is fully blocked by TTX and Picrotoxin, and it is slightly but significantly increased by Chlordiazepoxide, clearly indicate the specific neuronal and GABA<sub>A</sub> receptor-dependent nature of the signal observed. We took advantage of these properties to highlight a novel form of inhibitory synaptic plasticity, characterized by a long-lasting increase of GABAergic strength following mGlu<sub>5</sub> and IP<sub>3</sub> receptors activation.

The remarkable heterogeneity of CA1 hippocampal interneurons in terms of morphology and electrophysiological properties together with the extensive functional coupling to pyramidal cells<sup>4,7</sup>, underline the importance of monitoring GABAergic inhibitory activity at different neuro-architectural levels, from single cells to local circuits. Single cell recordings are valuable tools because of their ability to uncover sub-cellular input-output

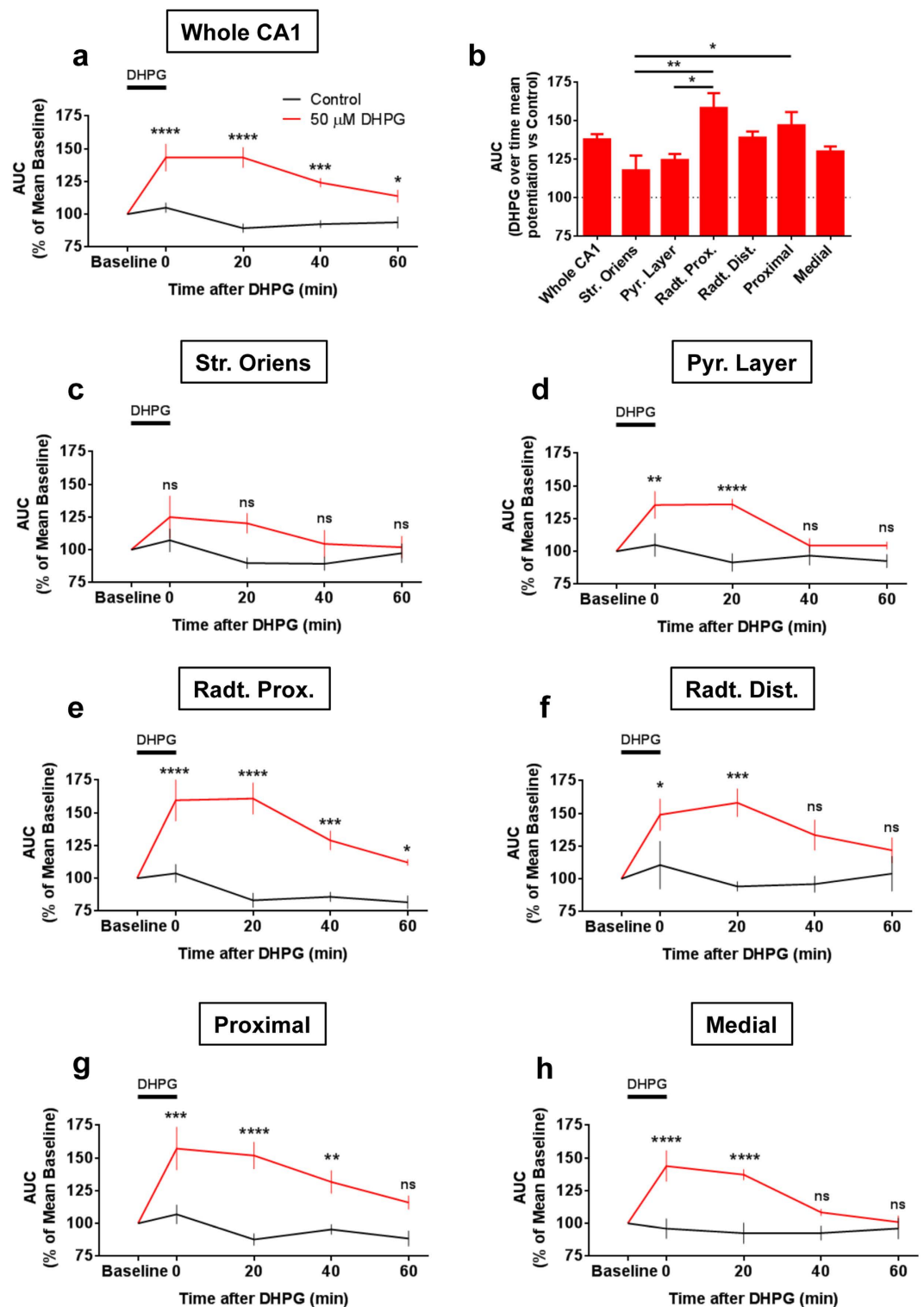


**Figure 4. Long-lasting increase of VSDI-recorded fIPSPs after group-I mGlu receptors activation.** Application of the selective group-I mGlu receptors agonist (S)-3,5-Dihydroxyphenylglycine (DHPG) for 10 minutes induces long-lasting enhancement of fIPSPs during the washout of the drug in the whole CA1 (a) and in its different sub-regions (c–h). (b) Graph showing mean over time percentage potentiation of DHPG vs control in whole CA1 and in its different sub-fields; one-way ANOVA followed by Tukey *post-hoc* test.  $n =$  (slices, mice): DHPG group = (7, 5), Control group = (7, 4). Data are mean  $\pm$  s.e.m. Statistical analysis in (a) and (c–h) is two-way ANOVA followed by Bonferroni *post-hoc* test. \* $p < 0.05$ , \*\* $p < 0.01$ , \*\*\* $p < 0.001$ , \*\*\*\* $p < 0.0001$ , ns = not significant.

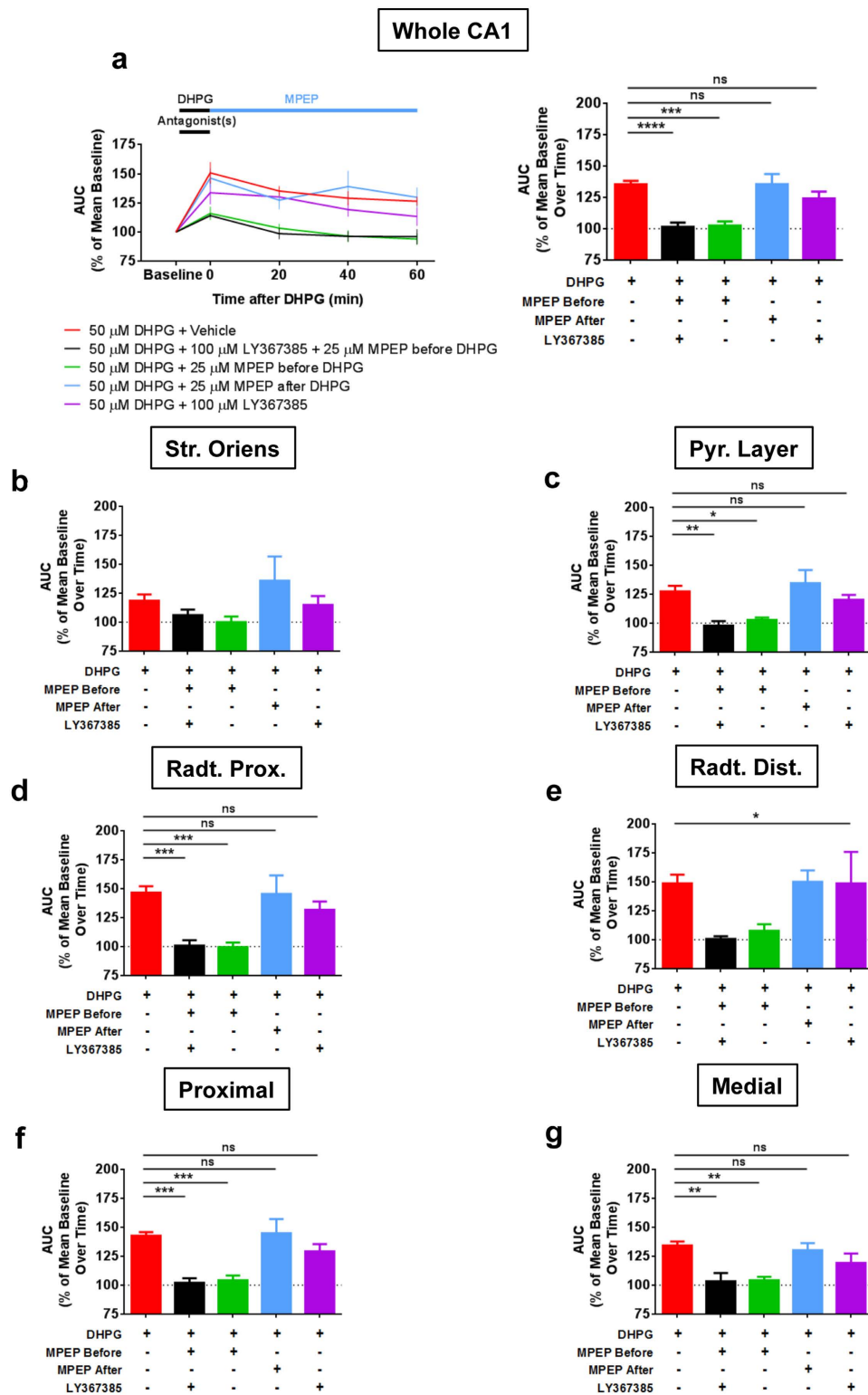


**Figure 5. Long-lasting increase of fIPSPs after DHPG application is mediated by mGlu<sub>5</sub> activation.** Slices were incubated with DHPG in presence of antagonists of group-I mGlu receptors (LY367385 for mGlu<sub>1</sub>, MPEP for mGlu<sub>5</sub> or both), which were kept until the end of DHPG application, except when MPEP has been applied after DHPG (represented in blue). In (a), left panel shows time course, while bars in right panel represent averaged drug effects over time. In (b–g), bars are the mean over time for each condition at the indicated region. One-way ANOVA followed by Dunnett *post-hoc* test has been used to assess differences between groups in (a) (right panel) and (b–g). In *radiatum* distal (e) there is a significant ANOVA ( $F_{(4,27)} = 2.912$ ,  $p = 0.04$ ) but not significant Dunnett's multiple comparisons test.  $n$  = (slices, mice): Vehicle group = (7, 7), LY367385 + MPEP before group = (7, 7), MPEP before group = (6, 5), MPEP after group (5, 4), LY367385 group = (7, 5). Data are mean  $\pm$  s.e.m. \*\* $p < 0.01$ , \*\*\* $p < 0.001$ , \*\*\*\* $p < 0.0001$ , ns = not significant.



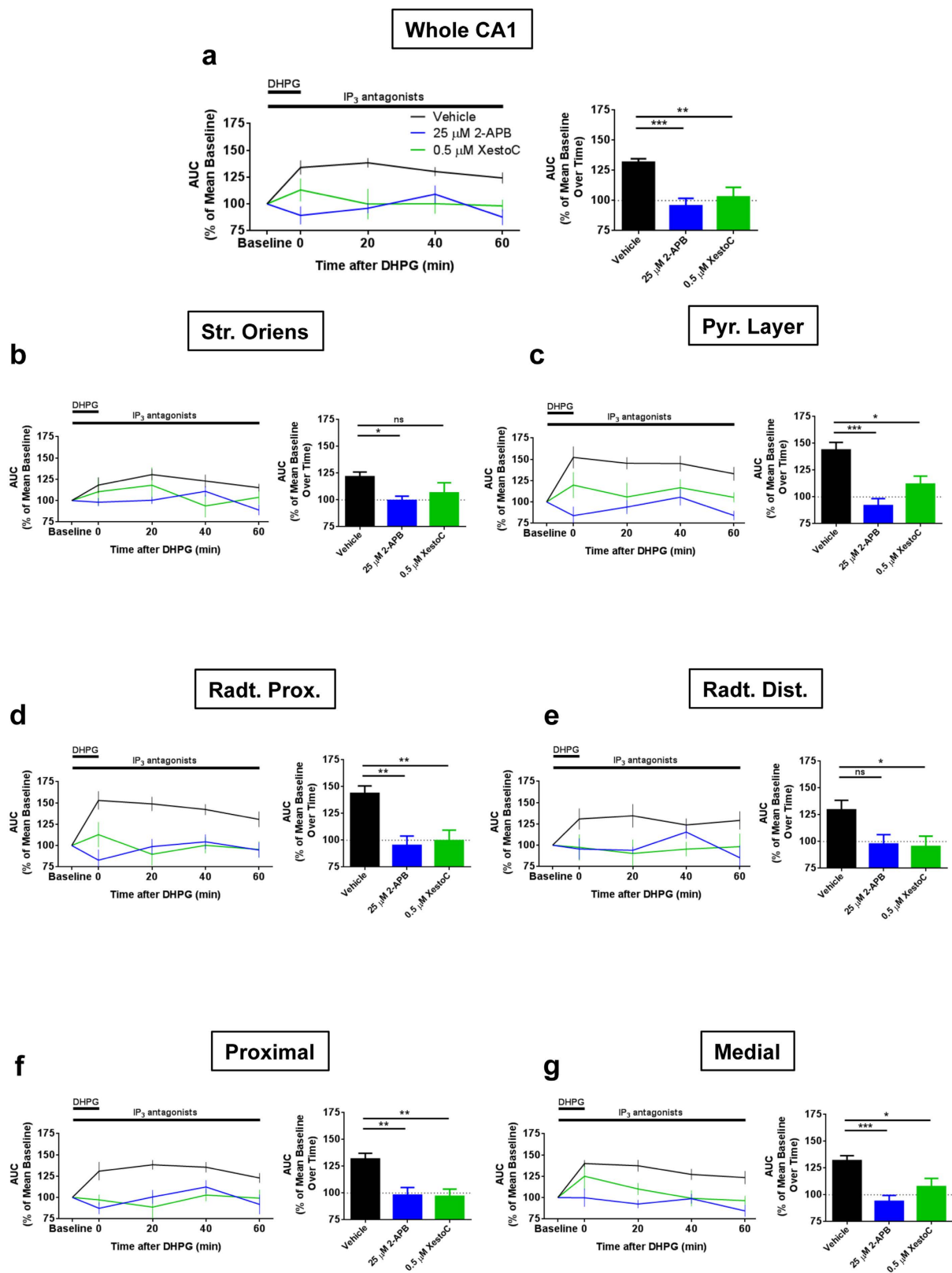


**Figure 6. Long-lasting increase of fIPSPs after DHPG application is mediated by IP<sub>3</sub> receptors activation.** DHPG failed to increase fIPSPs in all CA1 (a) and specifically in its different sub-regions (b–g) in presence of the cell-permeable IP<sub>3</sub> receptors blockers 2-APB or Xestospingon C (XestoC). In all figures, left panel shows the time course, while right panel is showing mean over time. Statistical analysis in right panel figures is one-way ANOVA followed by Dunnett *post-hoc* test. Vehicles of both IP<sub>3</sub> receptors antagonists have been pooled together since they are not different. n = (slices, mice): Vehicle group = (11, 9), 2-APB group = (5, 5), Xestospingon C group (5, 3). Data are mean ± s.e.m. \*p < 0.05, \*\*p < 0.01, \*\*\*p < 0.001, ns = not significant.

relationships and plasticity processes, but these approaches intrinsically lack the possibility to detect inhibitory transmission at larger network level, which can only be extrapolated, but not directly observed, from the data obtained. Very few attempts have been made to record network GABAergic activity<sup>16–18</sup>. In all these studies, single or few recording electrodes were used, thereby limiting the spatial information obtained about the GABAergic activity at network level.

In this context, our data reveal the possibility to study network GABAergic activity in large brain regions.

The presence of blockers of ionotropic glutamatergic transmission excludes synaptic activation of interneurons by glutamate released after Schaffer's collaterals stimulation, and suggests that the observed phenomenon is likely mediated by direct recruitment of interneurons, leading to synchronous release of GABA in an action potential dependent manner. Indeed, this is strengthened by the fact that minimal stimulation intensity is sufficient to engage significant interneuron population.

In the mature brain GABA, by acting on ionotropic GABA<sub>A</sub> receptors, inhibits excitation *via* two main mechanisms: hyperpolarization and shunting inhibition<sup>1</sup>. In our VSDI experiments, only hyperpolarization can be observed. Recent data, however, suggest that in the CA1 hippocampal region the hyperpolarizing component of GABA<sub>A</sub> receptor activity might be preponderant<sup>10</sup>. Nevertheless, we cannot exclude the presence of GABA<sub>A</sub> receptor shunting inhibition, which depends on the membrane potential state. These undetected events, however, would cause an underestimation of the GABAergic activity observed by VSDI recordings, further underlining the reliability of the approach.

Our data reveal a novel form of mGlu<sub>5</sub>-dependent plasticity of fIPSPs. In the hippocampal CA1 region, mGlu<sub>1</sub> and mGlu<sub>5</sub> are predominantly postsynaptic<sup>42</sup>. Whereas mGlu<sub>1</sub> is mainly expressed in interneurons, and primarily those present in *alveus* and *stratum oriens*, mGlu<sub>5</sub> is more widely present throughout the CA1, including the somatodendritic field of pyramidal cells, several classes of interneurons, and astrocytes<sup>25,42</sup>. Group-I mGlu receptors have a strong impact on neuronal activity by modulating cationic conductances, synaptic transmission and plasticity<sup>27</sup>. It is widely documented that activation of group-I mGlu receptors increases the excitability of hippocampal neurons<sup>27,37–40</sup>. In particular, mGlu<sub>1</sub> activation has been shown to trigger a direct depolarization of pyramidal cells, while mGlu<sub>5</sub> mediates a decrease of the slow after-hyperpolarization and a potentiation of NMDA currents<sup>34</sup>. Our data provide an additional effect to mGlu<sub>5</sub> activation (potentiation of fIPSPs), which will have to be considered in further studies on group-I mGlu-mediated synaptic and plasticity events. The study of specific group-I mGlu receptors signaling on GABAergic activity in hippocampal CA1 has to date been restricted to single cell resolution<sup>33,34,36,39,40</sup>, with currently no data about network inhibitory activity. Interestingly, however, Gereau *et al.*<sup>33</sup>, showed that activation of group-I mGlu receptors by DHPG increases the frequency and not the amplitude of spontaneous IPSC recorded from pyramidal cells, suggesting an increase of GABA release by interneurons excited by the agonist. In addition, van Hooft and colleagues<sup>36</sup> show that group-I mGlu receptors activation in several classes of *oriens-alveus* interneurons induces a dramatic increase of spike frequency and appearance of an inward current, consistent with group-I mGlu-induced increase of interneuron excitability. Furthermore, group-I mGlu receptor mediated increase in both interneuron excitability and/or GABA release, is not exclusive to the hippocampal CA1 region, but has also been reported in the thalamocortical neurons of dorsal lateral geniculate nucleus<sup>43</sup>, the ventral pallidum<sup>44</sup>, the periaqueductal grey<sup>45</sup>, retinal amacrine cells<sup>46</sup>, and in the entorhinal cortex<sup>47</sup>. These studies, however, show only a transient effect of DHPG on the electrophysiological activity of interneurons, which rapidly recovered to pre-drug conditions after washout of the compound. When we applied DHPG and recorded network GABA<sub>A</sub> receptor-mediated activity in the CA1 using VSDI, we found that mGlu<sub>5</sub> mediates a persistent enhancement of the signal that lasted for approximately 40–60 minutes after washout of the drug. Importantly, this effect is not attributable to a lack of drug washout, because the blockade of mGlu<sub>5</sub> receptors after DHPG application still triggers long-lasting potentiation of fIPSPs. Therefore, our present data are in agreement with previous studies performed at single cell level and, in addition, show that the exciting effect of mGlu<sub>5</sub> activation on inhibitory potentials induces phenomena of long-lasting plasticity when examined at network level. The differences in the duration of the stimulatory effects of mGlu<sub>5</sub> on GABAergic functions between single cell studies and the here described network level may be ascribed to the perturbation of intracellular composition due to the patch clamp procedure. Indeed, this may be suggested by a recent paper<sup>48</sup> demonstrating that mGlu receptors signaling in CA1 pyramidal cells is very sensitive to cytoplasmic dialysis, because using high resistance recording pipettes dramatically increases the amplitude and the duration of mGlu-mediated long-term depression of excitatory transmission. Future studies will investigate the role of intracellular dialysis in the short-to-long terms effects of mGlu<sub>5</sub> signaling on GABA<sub>A</sub> receptor activity.

The degree of the enhancement is region-specific inside the CA1, being generally more accentuated in the proximal part of *stratum radiatum* and in the region closer to the stimulation electrode, and weaker in the *stratum oriens* and in the pyramidal layer. The reasons for these differences are currently unknown. They could be related to the coincidence of interneuron activity in areas close to the stimulation, but they could also depend upon intrinsic differences between GABAergic network activities in different CA1 sub-fields. For instance, despite the fact that fIPSPs amplitude in the *stratum oriens* is comparable to other CA1 sub-layers, and that mGlu<sub>5</sub> receptors are abundantly expressed in this sub-region<sup>49</sup>, this layer seems to be less sensitive to DHPG-induced potentiation of fIPSPs. Importantly, our data also show that the activation of IP<sub>3</sub> receptors is a necessary step for mGlu<sub>5</sub>-induced potentiation of fIPSPs. Anatomical data<sup>50,51</sup> indicate that IP<sub>3</sub> receptors are less abundant in the *stratum oriens* than in other CA1 hippocampal layers (e.g. pyramidal layer and *stratum radiatum*), suggesting that the lower effect of DHPG in this sub-region might be due to the lower expression of key signaling elements downstream of mGlu<sub>5</sub>. The use of VSDI to study fIPSPs will allow future studies aimed at the precise anatomical, cellular, and molecular dissection of the plastic regulation of inhibitory transmission at the network level. For instance, given the growing body of literature suggesting that astrocytes are active regulators of GABAergic transmission<sup>52–54</sup>, it will be very interesting to address the role of these cell types in the regulation of fIPSPs.

Both mGlu<sub>5</sub> and inhibitory transmission are involved in important central pathologies, such as, among others, epilepsy and Fragile X Syndrome<sup>55–58</sup>. The possibility to study GABAergic transmission at the network level provides an additional tool for a better understanding of brain function in physiological and pathological conditions. For instance, Deng and co-workers<sup>47</sup>, showed that high glutamate levels, such as in epilepsy, increase the frequency and amplitude of spontaneous IPSCs recorded on principal neurons of the entorhinal cortex, an effect that is mediated by mGlu<sub>5</sub>. In light of these results, we could speculate that in the case of intense glutamatergic activity, as occurs during a seizure, glutamate spillover may activate peri-synaptic mGlu<sub>5</sub> receptors leading to a compensatory increase of network GABAergic activity. Interestingly, Campanac *et al.*<sup>59</sup> shows a persistent increase of inhibitory potentials recorded in CA1 pyramidal neurons after high-frequency stimulation of Schaffer's collaterals, an effect mediated by a long-term increase in the intrinsic excitability of parvalbumin-positive basket cells (PV<sup>+</sup>-BCs), and due to synaptic activation of mGlu<sub>5</sub> receptors. It would be interesting to explore in future studies the role of PV<sup>+</sup>-BCs, and other interneurons populations, in the mGlu<sub>5</sub>-induced long-lasting potentiation reported here. Likewise, future experiments will address the physiological implications of these pharmacological results, by testing whether different inductions protocols triggering the release of endogenous glutamate might also induce similar effects as DHPG.

Collectively, our data show that VSDI allows the detection and quantification of *bona fide* inhibitory network activity, and highlight the tight neuromodulatory coupling of excitation and inhibition at mesoscale level.

## Methods

**Slice preparation and staining with voltage sensitive dye.** Experiments were approved by and carried out according to the local ethical committee of the University of Bordeaux (approval number 501350-A) and the French Ministry of Agriculture and Forestry (authorization number 3306369).

8 to 11 weeks-old male C57BL/6-N mice (Janvier, France) were kept with *ad libitum* access to food and water, with 12 hours dark/light cycle (8 h00 pm/am).

Mice were decapitated after isoflurane anesthesia and 350 μm-thick sagittal slices containing dorsal hippocampus were cut with a vibratome (VT1200S, Leica, Germany).

During this procedure, the brain was immersed in ice-cold sucrose-based cutting solution bubbled with carbogen gas (95% O<sub>2</sub>/5% CO<sub>2</sub>) containing (in millimolar): 180 sucrose, 2.5 KCl, 26 NaHCO<sub>3</sub>, 1.25 NaH<sub>2</sub>PO<sub>4</sub>, 11 Glucose, 0.2 CaCl<sub>2</sub>, 12 MgCl<sub>2</sub>. After preparation, slices were transferred and incubated for 30 minutes at 34 °C in oxygenated artificial cerebrospinal fluid (ACSF) containing (in millimolar): 123 NaCl, 2.5 KCl, 26 NaHCO<sub>3</sub>, 1.25 NaH<sub>2</sub>PO<sub>4</sub>, 11 Glucose, 2.5 CaCl<sub>2</sub>, 1.3 MgCl<sub>2</sub> and then allowed to recover at room temperature in the same solution for at least 30 minutes before the staining procedure with the dye. Each slice was stained for 15 minutes in ACSF, under continuous carbogen flow, with the voltage sensitive fluorescent dye Di-4-ANEPPS (Sigma-Aldrich, France) at a concentration of 16.4 μM in DMSO (DMSO <0.1%).

The stained slice was then left to recover for at least 45 minutes, in dye-free ACSF at room temperature, before recordings. Mennerick *et al.*<sup>60</sup> found that Di-4-ANEPPS increases GABA<sub>A</sub> receptor conductance which is associated with a decreased network spontaneous spiking activity in dissociated cultures of hippocampal neurons. However, the effects reported are completely reversible to baseline level after washout of the cultures with dye-free solution and therefore exclude the impact of Di-4-ANEPPS-induced modulation of GABAergic activity on our VSDI recordings.

**Optical recording method.** Slices were placed in a recording chamber (Membrane Chamber; Scientific Systems Design Inc., Canada) under constant oxygenated ACSF flow (~2 ml/min) at room temperature.

To record neuronal signals with VSDI we used an epifluorescence microscope (Brainvision, Japan) equipped with the MiCAM02 optical imaging system (MiCAM02–HR; Brainvision, Japan) with a spatial resolution of 33.3 × 37.5 μm (horizontal and vertical, respectively) for each pixel.

A stereoscopic microscope (Leica, Germany) was used to visually guide the stimulating concentric bipolar electrode (FHC Inc., USA, catalog number CBARC75) into the proximal (respect to CA3) part of *stratum radiatum* to activate the Schaffer's collateral pathway. To improve the signal-to-noise ratio of the GABA<sub>A</sub> receptor-mediated hyperpolarization, for all the experiments, we set stimulation intensity at the maximum of the Input-Output curve (20 Volts, Fig. 2a) with a duration of 200 μs each stimulus, using an isolated voltage stimulator (DS2A, Digitimer Ltd., United Kingdom).

One acquisition consisted of 256 frames sampled every 2.2 ms, averaged 15 times at a time interval of 5 seconds (acquisition duration is ~70 seconds).

In experiments with DHPG, we performed six acquisitions as baseline, we then applied DHPG for ten minutes and finally we performed thirteen acquisitions during washout of DHPG, with an acquisition interval of 4 minutes.

In all experiments, before application of blockers of ionotropic glutamatergic transmission, one acquisition was taken in drug-free ACSF to check for slice health.

**Data analysis.** To quantify VSDI signals we calculated the fractional change in fluorescence ( $\Delta F/F^{-1}$ ) and we spatially smoothed the  $\Delta F/F^{-1}$  values with a 3 × 3 spatial filter using the image analysis-acquisition software (Brainvision, Japan). Exclusively for Supplementary Videos S1, S2 and S3, we used a spatial filter of 5 × 5 pixels, after  $\Delta F/F^{-1}$  signal normalization. In Fig. 1a,d,g and Supplementary Videos S1, S2 and S3 we isolated the CA1 region with a region of interest (ROI) by zeroing smoothed  $\Delta F/F^{-1}$  values outside the ROI.

A depolarization produces a reduction in fluorescence emitted by Di-4-ANEPPS, while a hyperpolarization an increase; therefore, for clarity,  $\Delta F/F^{-1}$  values representing depolarization (Fig. 1b,e) were considered positive.

ROIs were *post-hoc* visually drawn onto the slice, according to the representative spatial arrangement as shown in Figs 1b,c and 3b,e, using the image analysis-acquisition software (Brainvision, Japan). All the possible has been

done to exactly match the ROI boundaries with anatomical landmarks. However, the large spatial resolution of our VSDI recordings together with the relatively large size of each pixel, make it difficult to create an exact anatomical sub-division inside the CA1 region and therefore, the ROI named “Radt. Distal” (*radiatum* distal) contain *stratum lacunosum-moleculare* as well, while the ROI named “Pyr. Layer” (Pyramidal Layer) may include very limited parts of *stratum oriens* and *stratum radiatum*.

To draw ROIs in *stratum radiatum*, we first defined the ROI “Radt. Prox” and then we moved it ventrally at a position adjacent of the previous one to obtain the ROI “Radt. Dist”. To design ROIs along the proximo-distal axis of the CA1 relative to the stimulation electrode (named “P = proximal”, “M = medial” and “D = distal”), we first drew the ROI “P”, which was then duplicated and moved distally at adjacent points to obtain the ROIs “M” and then “D”. For the quantification of hyperpolarization signal across the sub-regions of CA1 (Fig. 3; schematic representation in b and e), we did as follows: at the middle of each dorso-ventral ROI (“str. Oriens”, “Pyr. Layer”, “Radt. Prox” and “Radt. Dist”) we drew a line (1 pixel wide, 8 pixels long) starting from the initial boundary relative to the stimulation electrode position. The same eight pixels long line was then positioned in the middle of each proximo-distal ROI (“P”, “M”, and “D”). To measure lengths along the proximo-distal axis of CA1 (Fig. 3f,g) we considered a pixel as a square of 35.4  $\mu\text{m}$  side, resulting from the mean of actual pixel size. A summary of all ROI sizes for experiments in Figs 1f, 2 and 4–6 and Supplementary Figs S1, S2 and S3 is available in the Supplementary Table S1.

To quantify GABA<sub>A</sub> receptor-mediated hyperpolarization recorded with VSDI we calculated the Area Under Curve (AUC) of traces representing mean  $\Delta F/F^{-1}$  values over time of each ROI, using a time interval of 200 milliseconds, starting from the time of hyperpolarization appearance (approximately 5 milliseconds after stimulus onset). To quantify depolarization signals in the presence of Picrotoxin (Fig. 1f and Supplementary Fig. S1), we calculated AUC values considering a time window of 30 milliseconds starting from the time point before stimulation. AUCs quantifications were performed with Axograph X (version 1.5, Axograph, USA).

Background AUC values (Figs 2b–e and 3c,d,f,g; Supplementary Fig. S2) were calculated measuring the AUC of traces from the same ROIs used for evaluation of signal of interest, which have been moved outside the hippocampus (in either cortex or thalamus). Final AUC values of background are the mean of three ROIs (except in Fig. 2b–e and Supplementary Fig. S2 where they are the mean of three ROIs for baseline and drug application, respectively).

In experiments with DHPG, “Baseline” is the mean of AUC values calculated for each ROI from the last four acquisitions before DHPG application. Except time “zero”, all others time points after DHPG are the mean of the AUC from four subsequent acquisitions. Data are then represented as percentage variation of mean AUC values with respect to mean baseline.

**Pharmacology.** 2,3-Dioxo-6-nitro-1,2,3,4-tetrahydrobenzo[f]quinoxaline-7-sulfonamide disodium salt (NBQX), D-(-)-2-Amino-5-phosphonopentanoic acid (APV), (S)-3,5-Dihydroxyphenylglycine (DHPG), (S)-(+)- $\alpha$ -Amino-4-carboxy-2-methylbenzeneacetic acid (LY367385), 2-Methyl-6-(phenylethynyl)pyridine hydrochloride (MPEP) were purchased from Abcam (France). Stock solutions of NBQX, D-APV, DHPG and MPEP were made in water, while LY367385 was dissolved in 100 mM of NaOH (final NaOH was ~0.1%). Once aliquoted, DHPG was used within one week. Slices were incubated with mGlu receptors antagonists from the start of the post-staining recovery period and, unless stated otherwise, until the end of DHPG application.

Octahydro-12-(hydroxymethyl)-2-imino-5,9:7,10a-dimethano-10aH-1,3]dioxocino[6,5-d]pyrimidine-4,7,10,11,12-pentol citrate (TTX), (2S)-3-[[[(1S)-1-(3,4-Dichlorophenyl)ethyl]amino-2-hydroxypropyl](phenylmethyl)phosphinic acid hydrochloride (CGP55845) and 2-Aminoethoxydiphenylborane (2-APB) were purchased from Tocris (United Kingdom). TTX was dissolved in water, while CGP55845 and 2-APB in DMSO (DMSO <0.1%). Xestospongine C was from Enzo Life Sciences (France) and dissolved in DMSO (DMSO <0.1%).

Picrotoxin (PTX) and 7-Chloro-2-(methylamino)-5-phenyl-3H-1,4-benzodiazepine 4-oxide hydrochloride (Chlordiazepoxide, CDP) were from Sigma-Aldrich (France). CDP was dissolved in water, while PTX in 100% ethanol. Drugs were bath-applied.

NBQX, APV and TTX were applied for 15 minutes, whereas PTX, CDP, and CGP55845 were applied for 30 minutes.

**Statistics.** Data are expressed as mean  $\pm$  s.e.m. All graphs and statistical analyses were performed with GraphPad Prism software (version 6.0). Two-tailed paired or unpaired t-test, one-way ANOVA, one-way repeated measures ANOVA, or two-way ANOVA followed by Tukey, Bonferroni or Dunnett *post-hoc* tests were used as appropriate. Differences were considered significant if  $p < 0.05$ .

## References

1. Fishell, G. & Rudy, B. Mechanisms of inhibition within the telencephalon: “where the wild things are”. *Annu Rev Neurosci* **34**, 535–67 (2011).
2. Bezaire, M. J. & Soltesz, I. Quantitative assessment of CA1 local circuits: knowledge base for interneuron-pyramidal cell connectivity. *Hippocampus* **23**, 751–85 (2013).
3. Aika, Y., Ren, J. Q., Kosaka, K. & Kosaka, T. Quantitative analysis of GABA-like-immunoreactive and parvalbumin-containing neurons in the CA1 region of the rat hippocampus using a stereological method, the disector. *Exp Brain Res* **99**, 267–76 (1994).
4. Freund, T. F. & Buzsáki, G. Interneurons of the hippocampus. *Hippocampus* **6**, 347–470 (1996).
5. Chamberland, S. & Topolnik, L. Inhibitory control of hippocampal inhibitory neurons. *Front Neurosci* **6**, 165 (2012).
6. Klausberger, T. & Somogyi, P. Neuronal diversity and temporal dynamics: the unity of hippocampal circuit operations. *Science* **321**, 53–7 (2008).
7. Petilla Interneuron Nomenclature, G. *et al.* Petilla terminology: nomenclature of features of GABAergic interneurons of the cerebral cortex. *Nat Rev Neurosci* **9**, 557–68 (2008).
8. Isaacson, J. S. & Scanziani, M. How inhibition shapes cortical activity. *Neuron* **72**, 231–43 (2011).
9. Kullmann, D. M. Interneuron networks in the hippocampus. *Curr Opin Neurobiol* **21**, 709–16 (2011).

10. Glickfeld, L. L., Roberts, J. D., Somogyi, P. & Scanziani, M. Interneurons hyperpolarize pyramidal cells along their entire somatodendritic axis. *Nat Neurosci* **12**, 21–3 (2009).
11. Buzsáki, G. Feed-forward inhibition in the hippocampal formation. *Prog Neurobiol* **22**, 131–53 (1984).
12. Freund, T. F. & Katona, I. Perisomatic inhibition. *Neuron* **56**, 33–42 (2007).
13. Pouille, F. & Scanziani, M. Enforcement of temporal fidelity in pyramidal cells by somatic feed-forward inhibition. *Science* **293**, 1159–63 (2001).
14. Cobb, S. R. *et al.* Synaptic effects of identified interneurons innervating both interneurons and pyramidal cells in the rat hippocampus. *Neuroscience* **79**, 629–48 (1997).
15. Sik, A., Penttonen, M., Ylinen, A. & Buzsáki, G. Hippocampal CA1 interneurons: an *in vivo* intracellular labeling study. *J Neurosci* **15**, 6651–65 (1995).
16. Arai, A., Silberg, J. & Lynch, G. Differences in the refractory properties of two distinct inhibitory circuitries in field CA1 of the hippocampus. *Brain Res* **704**, 298–306 (1995).
17. Bazélot, M., Dinocourt, C., Cohen, I. & Miles, R. Unitary inhibitory field potentials in the CA3 region of rat hippocampus. *J Physiol* **588**, 2077–90 (2010).
18. Lambert, N. A., Borroni, A. M., Grover, L. M. & Teyler, T. J. Hyperpolarizing and depolarizing GABAA receptor-mediated dendritic inhibition in area CA1 of the rat hippocampus. *J Neurophysiol* **66**, 1538–48 (1991).
19. Chemla, S. & Chavane, F. Voltage-sensitive dye imaging: Technique review and models. *J Physiol Paris* **104**, 40–50 (2010).
20. Peterka, D. S., Takahashi, H. & Yuste, R. Imaging voltage in neurons. *Neuron* **69**, 9–21 (2011).
21. Loew, L. M. *et al.* A naphthyl analog of the aminostyryl pyridinium class of potentiometric membrane dyes shows consistent sensitivity in a variety of tissue, cell, and model membrane preparations. *J Membr Biol* **130**, 1–10 (1992).
22. Grinvald, A., Mankner, A. & Segal, M. Visualization of the spread of electrical activity in rat hippocampal slices by voltage-sensitive optical probes. *J Physiol* **333**, 269–91 (1982).
23. Tominaga, T., Tominaga, Y., Yamada, H., Matsumoto, G. & Ichikawa, M. Quantification of optical signals with electrophysiological signals in neural activities of Di-4-ANEPPS stained rat hippocampal slices. *J Neurosci Methods* **102**, 11–23 (2000).
24. Canepari, M., Willadt, S., Zecevic, D. & Vogt, K. E. Imaging inhibitory synaptic potentials using voltage sensitive dyes. *Biophys J* **98**, 2032–40 (2010).
25. Ferraguti, F., Crepaldi, L. & Nicoletti, F. Metabotropic glutamate 1 receptor: current concepts and perspectives. *Pharmacol Rev* **60**, 536–81 (2008).
26. Fagni, L., Chavis, P., Ango, F. & Bockaert, J. Complex interactions between mGluRs, intracellular Ca<sup>2+</sup> stores and ion channels in neurons. *Trends Neurosci* **23**, 80–8 (2000).
27. Anwyl, R. Metabotropic glutamate receptors: electrophysiological properties and role in plasticity. *Brain Res Brain Res Rev* **29**, 83–120 (1999).
28. Castillo, P. E., Chiu, C. Q. & Carroll, R. C. Long-term plasticity at inhibitory synapses. *Curr Opin Neurobiol* **21**, 328–38 (2011).
29. Mann, E. O., Tominaga, T., Ichikawa, M. & Greenfield, S. A. Cholinergic modulation of the spatiotemporal pattern of hippocampal activity *in vitro*. *Neuropharmacology* **48**, 118–33 (2005).
30. Megias, M., Emri, Z., Freund, T. F. & Gulyás, A. I. Total number and distribution of inhibitory and excitatory synapses on hippocampal CA1 pyramidal cells. *Neuroscience* **102**, 527–40 (2001).
31. Davies, C. H., Davies, S. N. & Collingridge, G. L. Paired-pulse depression of monosynaptic GABA-mediated inhibitory postsynaptic responses in rat hippocampus. *J Physiol* **424**, 513–31 (1990).
32. Luscher, C. & Huber, K. M. Group 1 mGluR-dependent synaptic long-term depression: mechanisms and implications for circuitry and disease. *Neuron* **65**, 445–59 (2010).
33. Gereau, R. W. t. & Conn, P. J. Multiple presynaptic metabotropic glutamate receptors modulate excitatory and inhibitory synaptic transmission in hippocampal area CA1. *J Neurosci* **15**, 6879–89 (1995).
34. Mannaioni, G., Marino, M. J., Valenti, O., Traynelis, S. F. & Conn, P. J. Metabotropic glutamate receptors 1 and 5 differentially regulate CA1 pyramidal cell function. *J Neurosci* **21**, 5925–34 (2001).
35. McBain, C. J., DiChiara, T. J. & Kauer, J. A. Activation of metabotropic glutamate receptors differentially affects two classes of hippocampal interneurons and potentiates excitatory synaptic transmission. *J Neurosci* **14**, 4433–45 (1994).
36. van Hooft, J. A., Giuffrida, R., Blatow, M. & Monyer, H. Differential expression of group I metabotropic glutamate receptors in functionally distinct hippocampal interneurons. *J Neurosci* **20**, 3544–51 (2000).
37. Miles, R. & Poncer, J. C. Metabotropic glutamate receptors mediate a post-tetanic excitation of guinea-pig hippocampal inhibitory neurones. *J Physiol* **463**, 461–73 (1993).
38. Poncer, J. C., Shinozaki, H. & Miles, R. Dual modulation of synaptic inhibition by distinct metabotropic glutamate receptors in the rat hippocampus. *J Physiol* **485** (Pt 1), 121–34 (1995).
39. Gee, C. E. & Lacaille, J. C. Group I metabotropic glutamate receptor actions in oriens/alveus interneurons of rat hippocampal CA1 region. *Brain Res* **1000**, 92–101 (2004).
40. Woodhall, G., Gee, C. E., Robitaille, R. & Lacaille, J. C. Membrane potential and intracellular Ca<sup>2+</sup> oscillations activated by mGluRs in hippocampal stratum oriens/alveus interneurons. *J Neurophysiol* **81**, 371–82 (1999).
41. Foskett, J. K., White, C., Cheung, K. H. & Mak, D. O. Inositol trisphosphate receptor Ca<sup>2+</sup> release channels. *Physiol Rev* **87**, 593–658 (2007).
42. Ferraguti, F. & Shigemoto, R. Metabotropic glutamate receptors. *Cell Tissue Res* **326**, 483–504 (2006).
43. Errington, A. C., Di Giovanni, G., Crunelli, V. & Cope, D. W. mGluR control of interneuron output regulates feedforward tonic GABAA inhibition in the visual thalamus. *J Neurosci* **31**, 8669–80 (2011).
44. Diaz-Cabiale, Z. *et al.* Metabotropic glutamate mGlu5 receptor-mediated modulation of the ventral striopallidal GABA pathway in rats. Interactions with adenosine A(2A) and dopamine D(2) receptors. *Neurosci Lett* **324**, 154–8 (2002).
45. de Novellis, V. *et al.* Group I metabotropic glutamate receptors modulate glutamate and gamma-aminobutyric acid release in the periaqueductal grey of rats. *Eur J Pharmacol* **462**, 73–81 (2003).
46. Hoffpauir, B. K. & Gleason, E. L. Activation of mGluR5 modulates GABA(A) receptor function in retinal amacrine cells. *J Neurophysiol* **88**, 1766–76 (2002).
47. Deng, P. Y., Xiao, Z. & Lei, S. Distinct modes of modulation of GABAergic transmission by Group I metabotropic glutamate receptors in rat entorhinal cortex. *Hippocampus* **20**, 980–93 (2010).
48. Fan, W., Ster, J. & Gerber, U. Activation conditions for the induction of metabotropic glutamate receptor-dependent long-term depression in hippocampal CA1 pyramidal cells. *J Neurosci* **30**, 1471–5 (2010).
49. Smialowska, M. *et al.* Effect of chronic imipramine or electroconvulsive shock on the expression of mGluR1a and mGluR5a immunoreactivity in rat brain hippocampus. *Neuropharmacology* **42**, 1016–23 (2002).
50. Hertle, D. N. & Yeckel, M. F. Distribution of inositol-1,4,5-trisphosphate receptor isoforms and ryanodine receptor isoforms during maturation of the rat hippocampus. *Neuroscience* **150**, 625–38 (2007).
51. Pieper, A. A. *et al.* Differential neuronal localizations and dynamics of phosphorylated and unphosphorylated type 1 inositol 1,4,5-trisphosphate receptors. *Neuroscience* **102**, 433–44 (2001).
52. Christian, C. A. & Huguenard, J. R. Astrocytes potentiate GABAergic transmission in the thalamic reticular nucleus via endozepine signaling. *Proc Natl Acad Sci USA* **110**, 20278–83 (2013).
53. Jo, S. *et al.* GABA from reactive astrocytes impairs memory in mouse models of Alzheimer's disease. *Nat Med* **20**, 886–96 (2014).

54. Yoon, B. E. *et al.* Glial GABA, synthesized by monoamine oxidase B, mediates tonic inhibition. *J Physiol* **592**, 4951–68 (2014).
55. Piers, T. M. *et al.* Translational Concepts of mGluR5 in Synaptic Diseases of the Brain. *Front Pharmacol* **3**, 199 (2012).
56. Bear, M. F., Huber, K. M. & Warren, S. T. The mGluR theory of fragile X mental retardation. *Trends Neurosci* **27**, 370–7 (2004).
57. D’Hulst, C. & Kooy, R. F. The GABAA receptor: a novel target for treatment of fragile X? *Trends Neurosci* **30**, 425–31 (2007).
58. Treiman, D. M. GABAergic mechanisms in epilepsy. *Epilepsia* **42** Suppl 3, 8–12 (2001).
59. Campanac, E. *et al.* Enhanced intrinsic excitability in basket cells maintains excitatory-inhibitory balance in hippocampal circuits. *Neuron* **77**, 712–22 (2013).
60. Mennerick, S. *et al.* Diverse voltage-sensitive dyes modulate GABAA receptor function. *J Neurosci* **30**, 2871–9 (2010).

## Acknowledgements

We thank Dr. Alberto Bacci, Dr. Mark Sherwood and Maxime Houtekamer for critical reading of the manuscript, Dr. Ilaria Belluomo for invaluable support and all the members of Marsicano’s lab for useful discussions. M.C. is part of the international PhD program in Neuropharmacology (University of Catania, Italy). This work was supported by INSERM (G.M., F.M.), EU-Fp7 (REPROBESITY, HEALTH-F2–2008–223713 and PAINCAGE, HEALTH-603191, G.M.), European Research Council (ENDOFOOD, ERC–2010–StG–260515, G.M.), Fondation pour la Recherche Medicale (FDT20140930853, M.C. and DRM20101220445, G.M.), Human Frontiers Science Program (G.M.), Region Aquitaine (G.M.), Agence Nationale de la Recherche (ANR Blanc NeuroNutriSens ANR-13-BSV4-0006, G.M. BRAIN ANR-10-LABX-0043, G.M., F.M.).

## Author Contributions

M.C. contributed to experimental design, performed experiments, interpreted the results and wrote the manuscript. G.T. and C.E.L. contributed to experimental design and performed experiments. F.D., G.M. and F.M. supervised the project, interpreted the results and wrote the manuscript.

## Additional Information

**Supplementary information** accompanies this paper at <http://www.nature.com/srep>

**Competing financial interests:** The authors declare no competing financial interests.

**How to cite this article:** Colavita, M. *et al.* Layer-specific potentiation of network GABAergic inhibition in the CA1 area of the hippocampus. *Sci. Rep.* **6**, 28454; doi: 10.1038/srep28454 (2016).



This work is licensed under a Creative Commons Attribution 4.0 International License. The images or other third party material in this article are included in the article’s Creative Commons license, unless indicated otherwise in the credit line; if the material is not included under the Creative Commons license, users will need to obtain permission from the license holder to reproduce the material. To view a copy of this license, visit <http://creativecommons.org/licenses/by/4.0/>